Chapter 3:

Strontium-Doped Manganese Sulfide Nanostructures: Synthesis, Characterization, and Advanced Energy Storage Applications

Afshan Sharif, Sami Ullah

DOI: 10.21467/books.186.3
Additional information is available at the end of the chapter

The growing global energy crisis and the environmental impacts of fossil fuel reliance have driven a shift toward sustainable energy storage systems. Transition metal sulfides have become strong candidates for next-generation pseudocapacitors because of their excellent electrical conductivity and mechanical stability compared to oxides. This chapter explores the synthesis and electrochemical improvement of Strontium (Sr)-doped Manganese Sulfide (MnS) nanostructures. Using a scalable and eco-friendly hydrothermal method, we produced a series of Sr-doped MnS samples with different dopant levels (0%, 1%, 3%, 5%, and 7%). Structural analysis with X-ray Diffraction (XRD) confirmed a stable cubic phase, with an increase in crystallite size from 20.86 nm to 22.16 nm after doping, due to lattice expansion from the larger ionic radius of Sr^{2+}. Morphological inspection showed spherical nanostructures that become more prominent as Sr content rises. Optical tests showed a gradual decrease in the bandgap from 4.11 eV to 3.96 eV, indicating improved electronic mobility. Notably, the 7% Sr-doped MnS electrode achieved a high specific capacitance of 1487 F/g at a scan rate of 5 mV/s, nearly doubling the performance of undoped MnS. ling the performance of pristine MnS. These findings emphasize the transformative potential of Sr-doping in customizing the electronic and electrochemical characteristics of MnS for advanced energy storage devices.

1. Introduction

The modern development of technology requires multifunctional semiconductor materials with the ability to simultaneously meet the growing requirements for optoelectronics, solar cells, environmental, and electrochemical energy storage systems. Traditional semiconductor materials have provided humanity with electronics and photonics; however, their application is limited by a specific set of characteristics inherent in each material, such as band structure, charge-carrier mobilities, mechanical robustness, and recombination of photoexcited electron-hole pairs. Therefore, great interest is in the design of nanostructured materials with the ability to precisely regulate the desired optical and electronic properties by controlling their composition, morphology, and defects [1-4].

Nanotechnology provides the opportunity to create new materials through the regulation of their shape, size, and crystalline structure at the nanometer scale. Semiconductor nanostructures differ from their bulk counterparts in quantum confinement effects, high surface-area-to-volume ratios, an abundance of surface-active sites, and unique electronic structure, providing possibilities for controlling their optical absorption,

ISBN: 978-81-998984-9-3

electrical conductivity, transfer properties, catalytic activity, and electrochemical characteristics [5]. These advantages make semiconductor nanomaterials one of the most promising directions in modern material science and nanotechnology for developing optoelectronic devices, photodetectors, solar cells, photocatalysts, sensors, Li-ion accumulators, supercapacitors, and hydrogen generators [6].

Transition metal chalcogenides (TMCs) are attractive materials for exploring nanotechnology because of their great diversity of crystal structure, electronic configuration, and physicochemical properties. This class of materials consists of transition metal elements and chalcogens (sulfur, selenium, tellurium) with a wide range of oxidation states. Therefore, it is possible to develop and design TMCs with a variety of electronic structures and physicochemical properties suitable for specific applications. In addition, TMCs have demonstrated excellent performance in optoelectronics, electrocatalysis, photocatalysis, sensing, and energy storage [7, 8].

Compared to conventional oxides, binary transition metal sulfides possess more excellent physicochemical properties, including electrical conductivity, ionic diffusion, optical absorption, and stability under applied potentials. These advantages open the way for their use in multifunctional electronic and optoelectronic devices [9]. Among transition metal sulfides, manganese sulfide (MnS) is recognized as one of the most promising materials due to its biocompatibility, low cost, availability, and semiconductor properties. MnS has a p-type semiconductor character and possesses a variety of polymorphic crystalline structures, among which cubic (α-MnS), hexagonal (β-MnS), and metastable γ-MnS are the most common [10, 11]. In particular, cubic MnS has drawn the attention of many researchers due to its stability and a direct wide band gap of about 3.1-3.7 eV, depending on the synthesis method, crystallinity, size, and measurement conditions [10-12].

These optical characteristics, along with good chemical stability, make MnS a promising candidate for optoelectronic applications, in particular UV photodetectors, optical sensors, photocatalysts, light-emitting diodes, and electrodes for energy storage devices. Moreover, MnS nanostructures exhibit fascinating properties resulting from the quantum confinement effect, specific surface effects, and the increased importance of defects in nanosized solids. In particular, reducing the particle size to the nanoscale significantly affects the optical absorption, carrier mobility, recombination mechanisms, dielectric function, and electrochemical properties of MnS. In addition, MnS nanoparticles have shorter diffusion paths for ions and charge carriers and provide a higher number of active sites on the surface for electrochemical processes. All these effects are of great importance for the functionality of optoelectronic devices and electrochemical capacitors [10-13].

However, like any other semiconductor, MnS has its shortcomings that limit its practical implementation. First, the wide band gap of MnS causes a decrease in the absorption coefficient, resulting in the inability to effectively utilize solar radiation. Another disadvantage of MnS is the rapid recombination of electron-hole pairs under UV irradiation, which leads to a decrease in photoconductivity. At the same time, the electrical conductivity of MnS is also relatively low for applications in electronics and optoelectronics. Therefore, the use of MnS as an electrode in supercapacitors suffers from moderate ionic conductivity and electrical

conductivity, resulting in a relatively low energy storage capacity [14-16]. To solve these problems, researchers are looking for ways to modify the structural, optical, and electrochemical properties of MnS. In particular, the solution of these problems is seen in the synthesis of MnS nanostructures with tailored morphology, heterostructures, defect-engineered surfaces, composite materials, and doped MnS. Among the various strategies for modifying the properties of MnS, doping of MnS with foreign atoms is one of the most promising methods for improving the characteristics of semiconductor nanomaterials [17, 18]. Doping allows to control the electronic structure of MnS, charge-carrier concentration, defect structure, and other characteristics, leading to the desired optical, electrical, and electrochemical properties [19].

In particular, the substitution of Mn^{2+} with alkaline earth metal ions (Ba^{2+}, Sr^{2+}, Ca^{2+}) makes it possible to regulate the defect structure, lattice strain, and electronic properties of MnS. Among the alkaline earth metals, strontium has a larger ionic radius (1.13 Å) compared to Mn^{2+} (0.83 Å) and has good chemical stability. The replacement of some of the Mn^{2+} ions with Sr^{2+} ions leads to local lattice strain and defects, which are decisive factors in the optical, electronic, and electrochemical properties of MnS. Thus, Sr doping of MnS can be an effective method for modifying the characteristics of this semiconductor [18, 20, 21].

In addition, the substitution of Mn^{2+} with Sr^{2+} can significantly impact the optical properties of MnS, such as the band gap energy. More specifically, the introduction of foreign ions, local lattice strain, and defects can lead to a decrease in the optical band gap of MnS. Another feature of Sr-doped MnS is the possibility of suppressing the recombination of photoexcited electron-hole pairs, which also has a positive effect on the optical properties. These factors are of great importance for applications in optoelectronics, in particular for photodetectors, solar cells, and photoelectrochemical cells [14, 22, 23].

The use of MnS in electrochemical energy storage devices is attractive due to the presence of multiple oxidation states (Mn^{2+}, Mn^{3+}, Mn^{4+}) of manganese ions, which allows realizing reversible faradaic processes during charge-discharge of the supercapacitor. The specific capacitance of MnS-based supercapacitors largely depends on the specific surface area of MnS, the number of active sites, and the ionic conductivity of the material. Sr doping of MnS can be an effective way to increase the specific capacitance of a supercapacitor by enhancing the ionic conductivity of the semiconductor and creating additional active sites for the electrochemical oxidation-reduction reactions [24-27].

The method of hydrothermal synthesis provides an opportunity to obtain MnS nanostructures with a given morphology and high crystallinity. It is a relatively simple and inexpensive method that allows obtaining high-quality nanomaterials with desired properties. In particular, hydrothermal treatment of MnS makes it possible to create favorable conditions for the doping process and obtain Sr-doped MnS nanoparticles with the desired characteristics [28, 29].

Thus, this chapter studies the synthesis and characterization of Sr-doped MnS nanostructures, obtained by hydrothermal synthesis. Particular attention is paid to the relationship between the Sr content in the composition of MnS and its crystal structure, morphology, optical properties, luminescence properties, vibrational properties, and electrochemical characteristics. In addition, the correlations between the structure and the properties of Sr-doped MnS were analyzed and proved. The results obtained in this study

will contribute to a better understanding of the effect of alkaline-earth metal doping on the properties of semiconductor materials and the use of doped MnS for the needs of optoelectronics and electrochemical energy storage.

2. Experimental Methodology

2.1 Material Selection and Chemical Design

High purity analytical grade reagents were used in order to achieve reproducibility, high crystallinity and phase purity while avoiding any impurities that might affect the electrochemical properties of MnS nanostructures. Manganese chloride tetrahydrate ($MnCl_2 \cdot 4H_2O$) was selected as the Mn^{2+} salt owing to its high solubility, complete dissociation and chemical stability. Sodium sulfide nonahydrate ($Na_2S \cdot 9H_2O$) was chosen as the sulfur source owing to its high solubility and controllable release of S^{2-} ions during hydrothermal conditions. The reaction between the sulfide ions and Mn^{2+} leads to the formation of MnS:

$$Mn^{2+} + S^{2-} \rightarrow MnS$$

The sulfide concentration controls the nucleation, particle size and crystal growth while its hydrolysis controls the solution pH and phase purity.

The dopant source for MnS was selected to be strontium nitrate ($Sr(NO_3)_2$). This was chosen since strontium ions (Sr^{2+}) have a higher ionic radius than Mn^{2+} ions but the same oxidation state. Hence, the introduction of lattice distortion is facilitated without any need for charge compensation. This improvement will boost ion transport and electrochemical activity. The optimal Sr content was selected for better performance without introducing lattice distortion or additional phases. Deionized water acted as the reaction solvent to avoid any interference due to dissolved ions and facilitate crystal growth control. Ethanol was chosen for washing purposes to avoid salt contamination, agglomeration of nanoparticles, and ensure the large surface area necessary for good electrochemical performance.

2.2 Hydrothermal Synthesis: Thermodynamic and Kinetic Factors

Hydrothermal synthesis is a popular route for producing crystalline nanomaterials due to the ability to obtain materials with a high level of purity, controllable morphology, and relatively low temperature. High temperature and autogenous pressure in a closed Teflon-liner autoclave increase the solubility of precursors, diffusion of ions, and crystal growth, providing uniform nucleation and improved crystallinity. Crystal growth takes place upon reaching the state of supersaturation of the solution, which leads to nucleation of MnS nanoparticles and subsequent crystal growth as the concentration of precursors decreases. The ratio of nucleation and growth affects the final size and morphology of particles.

During synthesis, Sr^{2+} ions replace Mn^{2+} ions occupying the lattice sites of MnS, which provides lattice distortion affecting the process of crystal growth, defect distribution, and the electronic structure. Optimization of hydrothermal conditions allows obtaining Sr doped MnS with the uniform distribution of dopants without losing phase purity and crystallinity.

2.3 Hydrothermal Synthesis of Sr-Doped MnS Nanostructures

Sr-doped MnS nanostructures were prepared by means of hydrothermal synthesis (**Figure 3.1**). Equal stoichiometric amounts of $MnCl_2 \cdot 4H_2O$ and $Na_2S \cdot 9H_2O$ were dissolved in deionized water and thoroughly

mixed by continuous stirring. In case of the doped samples, $Sr(NO_3)_2$ was added to the manganese solution in the concentration of 1, 3, 5, and 7 wt.% prior to sulfur addition. The resulting mixture was stirred for 45 min to achieve homogenous ion distribution and the incorporation of Sr ions into the MnS lattice. The prepared precursor solution was introduced into the Teflon-lined autoclave (100 mL, 70% filling rate) and kept at the temperature of 180°C for 15 hours. Under hydrothermal conditions, increased ion solubility and diffusion led to the precipitation of MnS according to the following reaction:

$$Mn^{2+} + S^{2-} \rightarrow MnS$$

Firstly, fast nucleation took place and further crystal growth proceeded due to decreasing supersaturation. In this process, substitution of Mn^{2+} by Sr^{2+} ions resulted in structural distortions that controlled crystal growth, decreased grains' size, and increased defects concentration. Such structural features were essential for the electrochemical activity of the material.

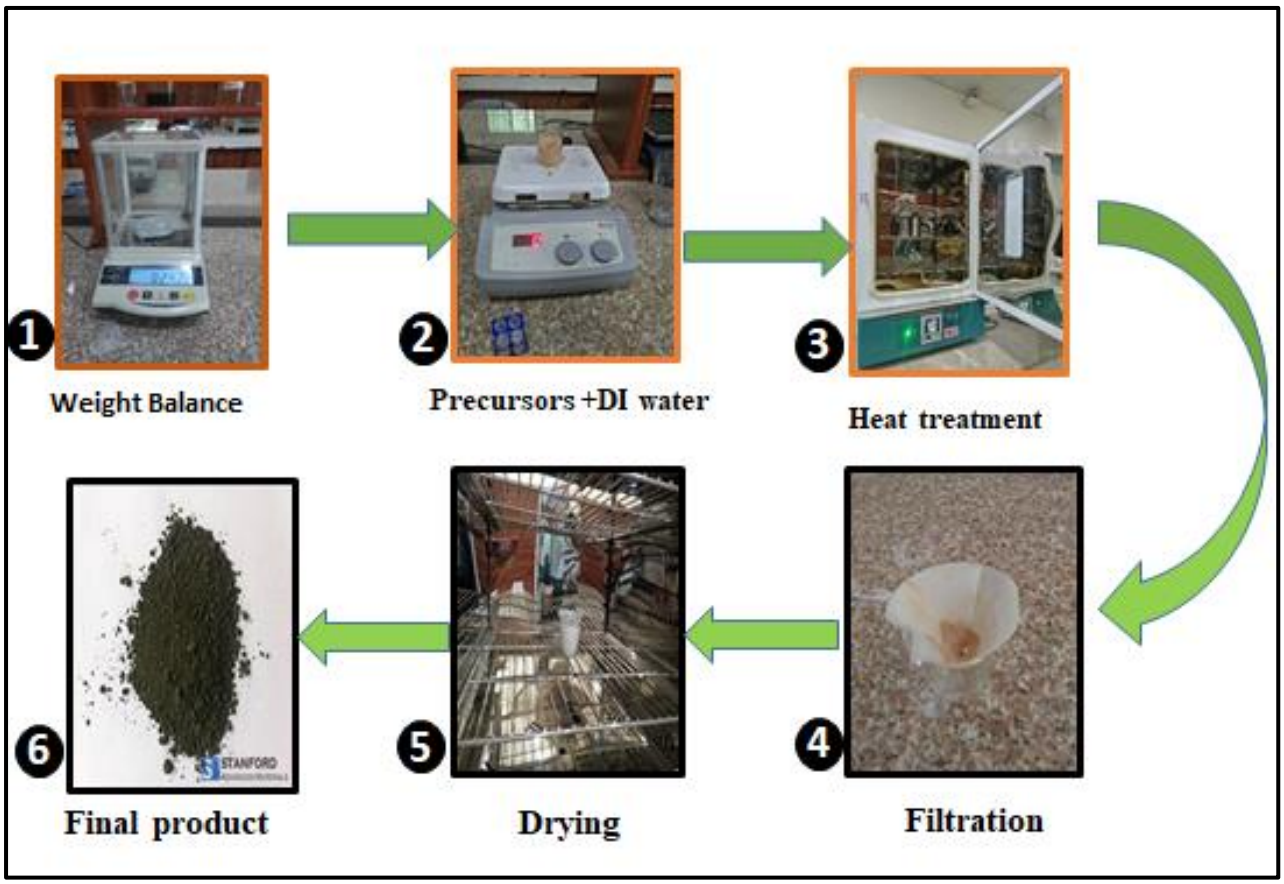

Figure 3.1 Flow diagram for preparation of Sr-doped MnS nanostructures.

The development of MnS nanostructures' morphology depends on the rate of nucleation and crystal growth that take place during the hydrothermal process. The growth of crystals is done by the continuous adsorption of Mn^{2+} and S^{2-} ions, and such processes as oriented attachment and Ostwald ripening affect particles' size and shape. The doping of Sr^{2+} ions affects crystal growth because of the introduction of lattice distortion, which produces smaller and more uniform nanoparticles with higher surface area and better ion transport. After the reaction, the autoclave was left to cool down to the room temperature naturally. This process decreases thermal stress, enhances crystallinity and stabilizes the crystal structure, providing good

ISBN: 978-81-998984-9-3

Book DOI: 10.21467/books.186

electrical conductivity and electrochemical stability. The precipitate was separated via centrifugation and washed multiple times with deionized water and ethanol to clean up the remaining by-products of the reaction, particularly sodium chloride, which is formed as follows:

$$MnCl_2 + Na_2S \rightarrow MnS + 2NaCl$$

The purified sample was dried under vacuum at 70°C for 12 hours to get rid of moisture while keeping the nanostructure intact.

2.4 Electrode Fabrication and Interface Engineering

The Sr-doped MnS electrodes were prepared to ensure effective electron transfer, high mechanical stability, and facile access of electrolyte to the electrode. The electrode was made up of the active material, carbon black, and PVDF as the binder supported by nickel foam to give high electrical conductivity and electrochemical performances. Sr-doped MnS, carbon black, and PVDF in a weight ratio of 80:10:10 were mixed. N-methyl-2-pyrrolidone (NMP) was added to form a homogenous slurry for a good dispersion of the active material and conductive additive. Nickel foam was chosen as the current collector for the high electrical conductivity, porous nature, and chemical stability in alkaline electrolytes. It was first cleaned using dilute HCl, deionized water, and ethanol before coating. The slurry was coated on nickel foam and then dried at 90°C for 24 h and compressed at 10 MPa. The obtained porous electrode ensured effective electron transport and electrolyte diffusion during electrochemical experiments.

2.5 Electrochemical Characterization and Cell Assembly

The electrochemical behavior of the Sr-doped MnS was studied by using a three-electrode setup, where Sr-doped MnS was used as the working electrode, Ag/AgCl as the reference electrode, and Pt wire as the counter electrode in 1.0 M KOH electrolyte. The electrochemical properties of the material were examined using cyclic voltammetry (CV), galvanostatic charge-discharge (GCD), and electrochemical impedance spectroscopy (EIS).

3. Results and Discussion

3.1 Morphological and Elemental Evolution (SEM & EDX)

The morphology of the surface of the electrode material defines the number of active sites for redox reactions to occur. As depicted in **Figure 3.2(a)** (SEM), the synthesized MnS has a morphology of spherical particles. When the content of Sr increases from 0% to 7%, the spherical nanostructures become better visible and more uniform **Figure 3.2(b)**. In the case of supercapacitors, it is a very valuable morphology; the spherical nanoparticles have a large surface area/volume ratio, which allows the electrolyte (KOH) to penetrate into them.

The elemental purity of the sample has been confirmed by using the Energy Dispersive X-ray (EDX) technique (**Figure 3.2(c, d)**). It is obvious that the obtained spectra show the presence of Manganese (Mn), Sulfur (S), and Strontium (Sr), but no impurities were found in the sample. This shows that the hydrothermal synthesis has successfully incorporated the Sr dopant into the MnS matrix.

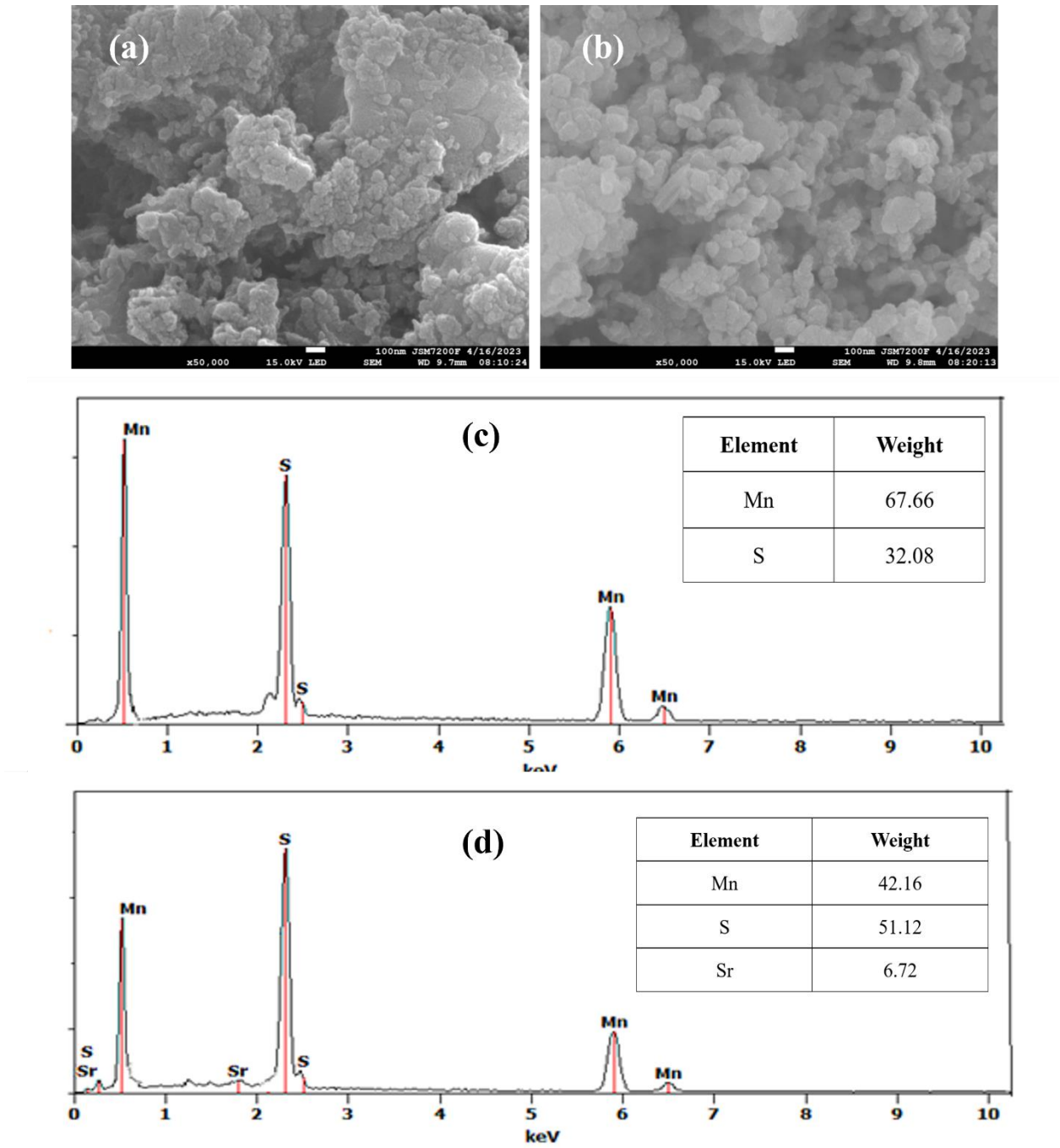

Figure 3.2 SEM images of (a) undoped MnS nanostructures and (b) 7% Sr-MnS nanostructures. EDX spectra of (c) undoped MnS nanostructures and (d) 7% Sr-MnS nanostructures.

3.2 Structural Analysis and Lattice Dynamics (XRD)

Crystalline structure and phase purity of the nanostructures produced were determined through X-ray Diffraction (XRD). As shown in **Figure 3.3(a, b)**, the diffraction patterns of the pristine and the Sr-doped MnS nanostructures show sharp and distinct peaks, which means the material is highly crystallized. Reflections at 2θ angles representing (111), (200), (220), (311), (222), and (400) planes are in perfect

ISBN: 978-81-998984-9-3

Book DOI: 10.21467/books.186

agreement with the **JCPDS card No. 06-0518**. This demonstrates that the stable face-centered cubic (FCC) phase has been formed. A careful analysis of the (200) peak provides important information about the lattice dynamics. After doping of Strontium, there is a shift of the diffraction peaks towards low 2θ angles **Figure 3.3(b)**. Based on Bragg's Law ($2d\sin\theta = n\lambda$), this means a smaller diffraction angle (θ) should be accompanied by increased interplanar distance (d). This lattice expansion is due to the huge difference between the ionic radii of the two species; the Sr^{2+} ion (1.13 Å) is 38% larger compared to the host Mn^{2+} ion (0.82 Å). In other words, when these large Strontium ions replace the Manganese ions, they create local compressive strain and enlarge the lattice.

The average crystallite size (D) was determined using Scherrer's equation ($D = K\lambda/\beta\cos\theta$), where the values increased systematically from 20.86 nm for MnS without doping to 22.16 nm for the 7% Sr doped compound (**Figure 3.3**). It can be said that Sr^{2+} ions serve as nuclei that affect the kinetics of the hydrothermal synthesis process. From the point of view of energy storage applications, the achieved structural change is revolutionizing. The lattice enlargement causes a greater lattice enlargement, thereby increasing the "corridors of diffusion" of electrolyte ions (OH^-). For efficient energy storage in supercapacitors, the process of ions' intercalation/deintercalation should occur almost barrier-free. By artificially "straining" the lattice of MnS, we have optimized its structure with respect to the resistance and capacity of the electrode material.

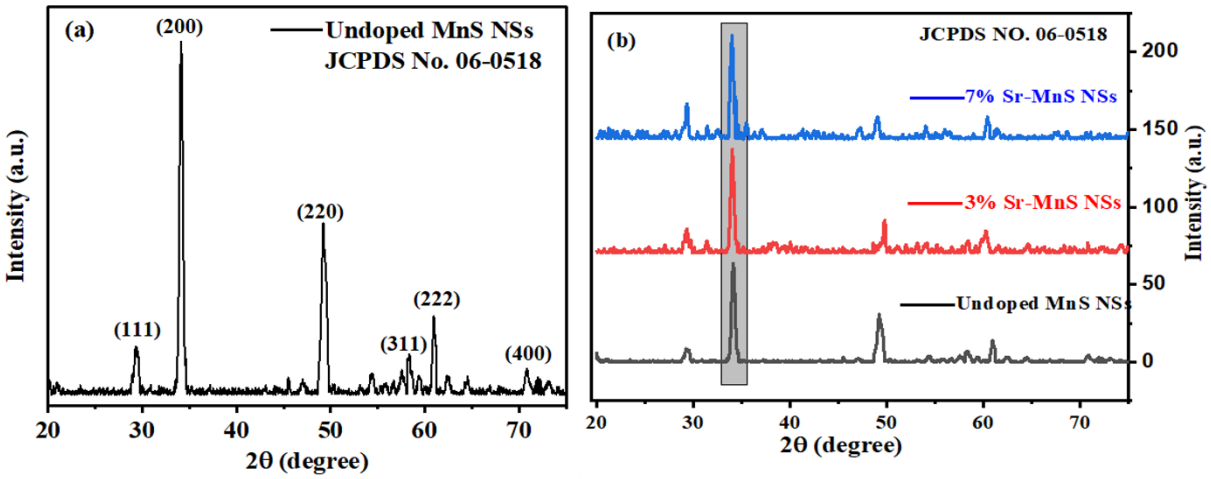

Figure 3.3 XRD patterns of a) Undoped MnS nanostructures, b) Undoped MnS, 3% and7% Sr-MnS nanostructures.

3.3 Electronic and Optical Modulation (UV-Vis, PL, and Raman Analysis)

Electron configuration in a semiconductor forms the basic factor for determining its conductance behavior and charge transfer dynamics. In the current work, the combined influence of Sr doping in the MnS material lattice was studied employing three spectroscopic methods, namely, UV-Visible Absorption, Photoluminescence (PL), and Raman Spectroscopy.

3.3.1 Bandgap Engineering and Conductivity (UV-Vis)

Absorption properties were used to investigate the direct bandgap (E_g) of the structures, which is an important value for electrochemical energy storage. **Figure 3.4** presents the calculated absorption spectra based on the Tauc's law:

$$(\alpha h\nu)^2 = A(h\nu - E_g)$$

where α is the absorption coefficient and hν is the energy of a photon.

The un-doped MnS possessed a large bandgap of 4.11 eV, which is typical of a semi-insulating material. A decrease in the bandgap value with the increase in the doping level was revealed; in particular, the 7% Sr-doped samples had a reduced bandgap of 3.96 eV **Figure 3.4(c)**. The "bandgap narrowing" effect can be caused by several reasons:

Intermediate Energy Levels: The presence of of Sr^{2+}ions introduces new electronic states in the forbidden zone of the host MnS material. These "tail states" connect the valence band (VB) and the conduction band (CB) making it easier for electrons to excite across this gap.

Lattice Strain: It is known from XRD analysis that the substitution of of $Mn^{2+}$by the bigger of Sr^{2+}leads to a considerable strain of the crystal lattice. The change in the orbital overlap causes the change in the density of states (DOS).

In terms of energy storage, this decrease in E_g is revolutionary. A small band gap means higher electronic conductivity in itself. In a supercapacitor, the electrode should be able to allow the fast flow of electrons to the current collector at high rates of discharge. The lower energy required to move electrons in the electrode, due to Sr-doping, makes the Equivalent Series Resistance (ESR) much lower.

ISBN: 978-81-998984-9-3

Book DOI: 10.21467/books.186

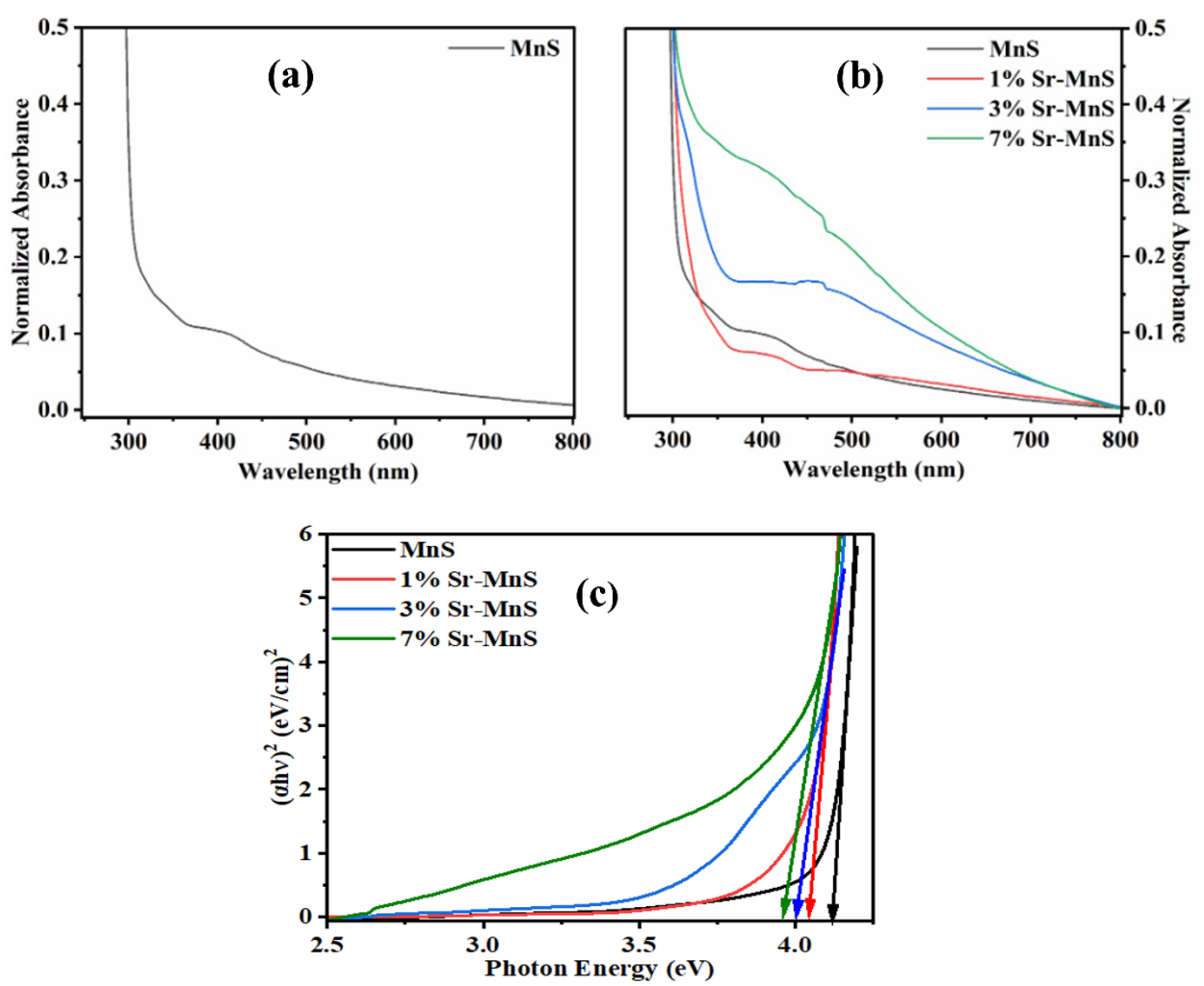

Figure 3.4 UV-absorption spectra of (a) Undoped MnS and (0, 1, 3, 5 and 7)% Sr-MnS nanostructures (b) and Energy band gap of as-synthesized Undoped MnS and (1,3,5 and 7)% Sr-MnS nanostructures.

3.3.2 Charge Carrier Dynamics and Recombination (PL)

The Photoluminescence technique sheds light on the recombination behavior of excited charge carriers; namely the recombination rates of electron-holes (e^-/h^+) pairs. As can be seen from **Figure 3.5(a),** the nanostructures of MnS demonstrate intense blue emission around 382 nm when excited by 330 nm light. This emission occurs mainly due to NBE transitions and recombination of electrons originating from sulfur vacancies to the valence band.

Another important result of this research is the quenching effect of PL intensity when increasing Strontium concentration (**Figure 3.5(b)**). From the perspective of energy storage, the high intensity of PL means that the charge carriers quickly recombine and lose their energy in the form of light emission. The quenching effect of PL intensity in the case of Sr-doped MnS reveals the fact that the Sr ion acts as an effective center of trapping charges or facilitator of separating the e^-/h^+ pairs. Instead of recombination of these charges, they get an opportunity to take part in faradaic redox reactions at the electrode-electrolyte interface. This

behavior is typical for a good pseudocapacitive material since only the maximum number of charges is used for energy storage.

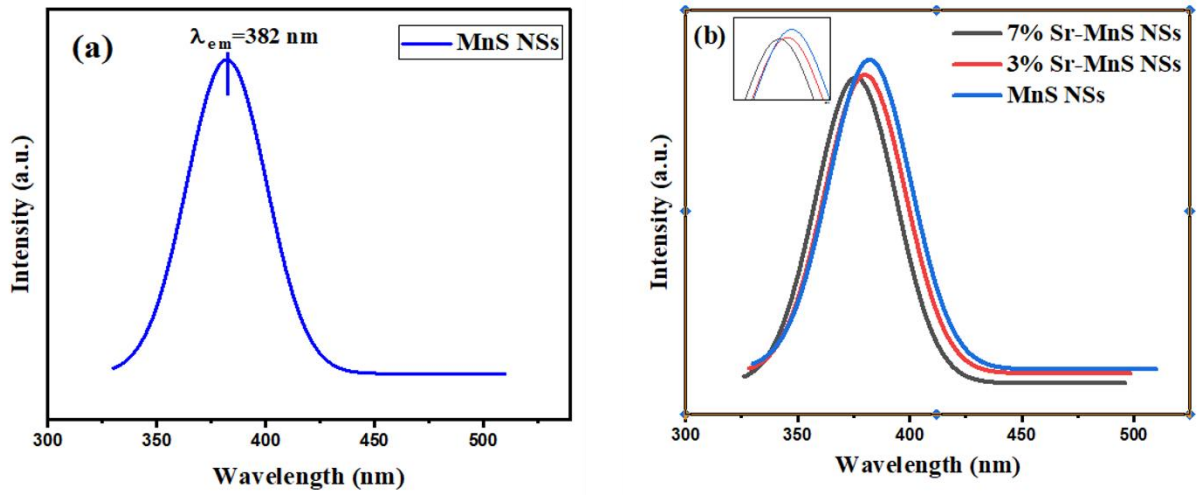

Figure 3.5 PL spectra of (a) Undoped MnS and (0, 3, and 7)% Sr-MnS nanostructures (b).

3.4 Electrochemical performance for supercapacitors

A thorough test of the suitability of Sr-doped Manganese Sulfide (MnS) as an energy storage material must include analysis of its electrochemical characteristics. The electrochemical performance was analyzed using the Cyclic Voltammetric method (CV) in a three-electrode setup with a 1.0 M KOH aqueous electrolyte solution. KOH electrolyte is optimal for Mn-based sulfides due to the need for redox reactions during pseudocapacitance.

3.4.1 Cyclic Voltammetry (CV) Profiles Analysis

The cyclic voltammetric curves of undoped MnS, 3% Sr-MnS and 7% Sr-MnS within the potential range from -0.2 to 0.6 V (total ΔV = 0.8 V) and at various scan rates from 5 mV/s to 75 mV/s (**Figures 3.6(a-c)**) all show the shape of quasi-rectangular CV curves with clear redox peaks – typical for pseudocapacitives. In contrast to Electric Double-Layer Capacitors (EDLCs) where the energy is stored via simple ion absorption, the pseudocapacitors based on Sr-MnS use reversible redox transitions of manganese ions ($Mn^{2+} \leftrightarrow Mn^{3+} \leftrightarrow Mn^{4+}$).

The other interesting feature seen from the CV curve is the considerable increase in the integrated area of the CV curves as the amount of Strontium increases. The 7% Sr doped MnS electrode has the largest integrated area due to its maximum charge storing capacity. This is because of the synergy of Strontium which improves the electrical environment of the electrode.

ISBN: 978-81-998984-9-3

Book DOI: 10.21467/books.186

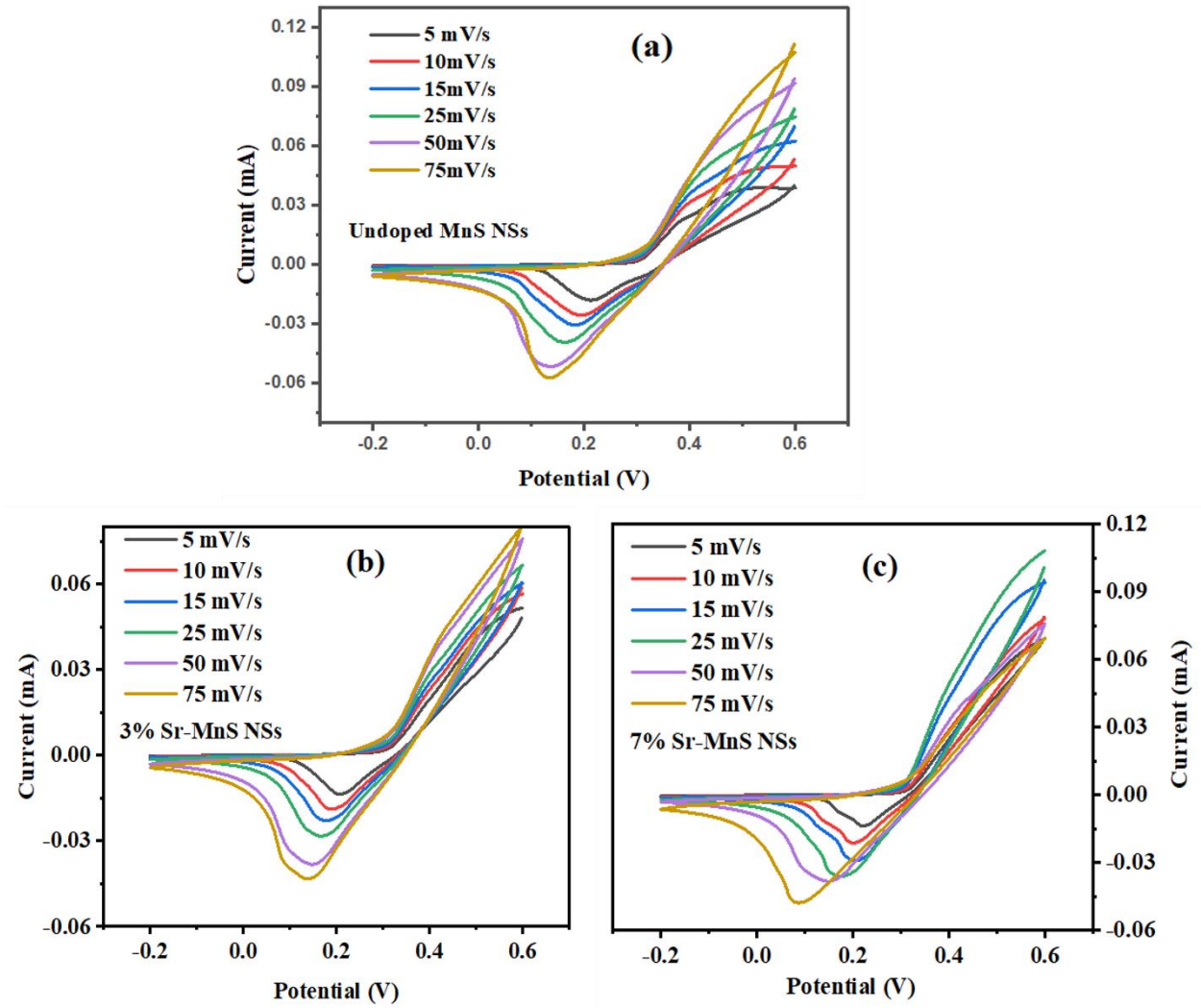

Figure 3.6 Cyclic Voltammetry at various scan rates of (a) Undoped MnS, (b) 3% Sr-MnS, and (c) 7% Sr-MnS nanostructures.

3.4.2 Quantitative Specific Capacitance (C_p) Evaluation

The specific capacitance was calculated using the relation:

$$C_p = \frac{A}{2Km\Delta V}$$

where K is the scan rate, m is the mass of the active material (2 mg), A is the integrated area of the CV curve, and ΔV is the potential window (0.8 V).

As can be seen in **Figure 3.6(c)**, there has been a remarkable enhancement in the energy storage capability when doped:

Pristine MnS: This material delivered a value of C_p of 776 F/g at 5 mV/s. Although decent for a transition metal sulfide, the performance of this material is hampered by internal resistance.

3% Sr-MnS: In this case, the C_p value was elevated to 1104 F/g, showing that only a small amount of Sr-doping helps charge storage.

7% Sr-MnS: This optimum electrode was capable of delivering an excellent specific capacitance of 1487 F/g at 5 mV/s.

This almost double the enhancement from that of the undoped version is really remarkable. This clearly shows that the optimal doping level of 7% Sr allows the nanostructure to have optimum lattice expansion and electronic conductivity to maximize participation of Manganese sites in the redox reaction.

3.4.3 Impact of Scan Rate and Rate Capability

Furthermore, the study examined the capacity as a function of scan rate from 5 to 75 mV/s. It has been seen that in all cases, the specific capacitance decreases with the increase in scan rate. For instance, the 7% Sr-MnS electrode moves from 1487 F/g at 5 mV/s to 190 F/g at 75 mV/s.

This is a typical feature of a diffusion controlled process. The OH^- ions present in the electrolyte have enough time to go inside the spherical nanomaterials and reach the active sites (bulk diffusion) when the scan rate is low (5 mV/s). When the scan rate increases, the ions can only react with the outermost part of the electrode material, resulting in decreased capacitance. However, the Sr-doped materials had a higher C_p value than undoped MnS at all scan rates, indicating that the formation of "open" lattices by Sr^{2+} ions (proven by XRD results) helps to transport the ions more efficiently.

3.4.4 The Mechanism of Enhancement: Why 7% Sr-MnS?

There are three converging factors responsible for the outstanding performance of 7% Sr doped MnS electrode:

Charge Transfer Resistance Reduction: Due to the reduction of band gap from 4.11 eV to 3.96 eV (UV-Vis), the quantity of charge carriers is increased, allowing electrons to quickly transfer from redox centers to Ni-foam current collector.

Ion Accessibility: Due to the presence of spheres in SEM and expanded lattice due to Sr doping proven by XRD, the "channels" in the crystal are broad enough for the OH^- ions to travel without steric hindrance.

Recombination Inhibition: It is proven by PL quenching that Sr serves as an agent inhibiting premature recombination of charge carriers, making sure the electrons are harvested from $MnS + OH^- \rightarrow MnSOH + e^-$ reaction.

To sum up, the 7% Sr-doped MnS nanostructure may serve as an efficient electrode material, solving problems of pristine MnS and providing opportunities for creating advanced supercapacitors for future technologies.

4. Conclusion and Future Perspectives

The research carried out in this chapter is a clear success in showing the profound effect of Sr doping on the structural and electrochemical properties of manganese sulfide nanomaterials. Using an eco-friendly

and scalable hydrothermal method, we have synthesized a top-notch electrode material which can mitigate the drawbacks associated with pure transition metal sulfides.

Conclusions drawn from this study are some important results that bring out a link between materials physics and energy engineering:

Structural Optimization: The cubic MnS formation has been successfully achieved with controlled lattice expansion caused by the doping of Sr. Lattice expansion resulting from increased ionic radius of Sr^{2+} leads to an increase in the crystallite size up to 22.16 nm compared to 20.86 nm, which results in a more stable and "open" structure for higher rates of ion movement.

Morphological Optimization: SEM results show a tendency to form more spherical structures due to Sr content increment. Such type of structure is beneficial for energy storage, since it provides more electroactive surface to interact with electrolyte.

Electronic Bandgap Engineering: An important result that should be mentioned in this study is the possibility to decrease the optical bandgap from 4.11 eV to 3.96 eV. Together with the quenching of photoluminescence, it is evident that Sr doping increases electronic conductivity and reduces charge carriers recombination, decreasing internal resistance of the resulting electrodes.

Electrochemical Benchmark Performance: The electrode consisting of 7% Sr-doped MnS was found to be the optimal combination, exhibiting an outstanding specific capacitance of 1487 F/g at 5 mV/s scan rate, demonstrating the importance of doping an element into manganese-based materials.

With the increased push towards electrification and clean energy grids on a global scale, the need for "battery-like" energy storage density along with "capacitor-like" power output has never been greater. The Sr-MnS nanostructures designed in this study serve as an example of how to combine both of these characteristics in a successful material. The use of cheap, Earth-abundant materials, such as Manganese and Strontium, demonstrates an environmentally friendly and economically efficient way to produce energy storage technologies.

5. Publisher's Note

AIJR remains neutral with regard to jurisdictional claims in published maps and institutional affiliations.

Author's Detail

Afshan Sharif, Sami Ullah*

Department of Physics, University of Okara, Okara, Pakistan.

*Corresponding author

How to Cite this Chapter:

A. Sharif, S. Ullah, "Strontium-Doped Manganese Sulfide Nanostructures: Synthesis, Characterization, and Advanced Energy Storage Applications," in *Emerging Functional Materials for a Sustainable Energy Future*, M. A. Kamran, Ed. India: AIJR Publisher, 2026, pp. 44-58. ISBN: 978-81-998984-9-3, doi: 10.21467/books.186.3

References

[1] S. Sze and K. Ng, "Chapter 3 Metal-Semiconductors Contacts," *Physics of Semiconductor Devices, 3rd ed.; John Wiley & Sons: Hoboken NJ, USA,* pp. 134-196, 2007.

[2] Y. Peter and M. Cardona, *Fundamentals of semiconductors: physics and materials properties*. Springer Science & Business Media, 2010.

[3] C. Burda, X. Chen, R. Narayanan, and M. A. El-Sayed, "Chemistry and properties of nanocrystals of different shapes," *Chemical reviews,* vol. 105, no. 4, pp. 1025-1102, 2005.
[4] S. Ullah, F. K. Butt, and J. Ahmad, "Importance of 2D Nanomaterials for Energy," in *Energy Applications of 2D Nanomaterials*: CRC Press, 2022, pp. 1-19.
[5] S. L. Brock, "Nanostructures and Nanomaterials: Synthesis, Properties and Applications By Guozhang Cao (University of Washington). Imperial College Press (distributed by World Scientific): London. 2004. xiv+ 434 pp. $78.00. ISBN 1-86094-415-9," ed: ACS Publications, 2004.
[6] A. Fujishima and K. Honda, "Electrochemical photolysis of water at a semiconductor electrode," *nature,* vol. 238, no. 5358, pp. 37-38, 1972.
[7] T. Heine, "Transition metal chalcogenides: ultrathin inorganic materials with tunable electronic properties," *Accounts of chemical research,* vol. 48, no. 1, pp. 65-72, 2015.
[8] J. H. Han, M. Kwak, Y. Kim, and J. Cheon, "Recent advances in the solution-based preparation of two-dimensional layered transition metal chalcogenide nanostructures," *Chemical reviews,* vol. 118, no. 13, pp. 6151-6188, 2018.
[9] S. Ali *et al.*, "Transition metal sulfides: From design strategies to environmental and energy-related applications," *Coordination Chemistry Reviews,* vol. 523, p. 216237, 2025.
[10] M. Saeed *et al.*, "Comprehensive reviews on the potential applications of inorganic metal sulfide nanostructures in biological, environmental, healthcare, and energy generation and storage," *Reviews in Inorganic Chemistry,* vol. 45, no. 2, pp. 237-274, 2025.
[11] J. Hu *et al.*, "Synthesis and electrochemical application of two-dimensional manganese-based materials," *Inorganic Chemistry Frontiers,* vol. 11, no. 15, pp. 4528-4551, 2024.
[12] J. Hu, Y. Zhou, Y. Liu, Z. Xu, and H. Li, "Recent advances in manganese-based materials for electrolytic water splitting," *International Journal of Molecular Sciences,* vol. 24, no. 7, p. 6861, 2023.
[13] C. Lokhande *et al.*, "Process and characterisation of chemical bath deposited manganese sulphide (MnS) thin films," *Thin Solid Films,* vol. 330, no. 2, pp. 70-75, 1998.
[14] A. M. Ferretti, S. Mondini, and A. Ponti, "Manganese sulfide (MnS) nanocrystals: synthesis, properties, and applications," *Adv. Colloid Sci,* vol. 10, no. 65092, p. 10.5772, 2016.
[15] M.-R. Gao, Y.-F. Xu, J. Jiang, and S.-H. Yu, "Nanostructured metal chalcogenides: synthesis, modification, and applications in energy conversion and storage devices," *Chemical Society Reviews,* vol. 42, no. 7, pp. 2986-3017, 2013.
[16] Z. Deng *et al.*, "Recent developments in manganese chalcogenide electrodes for sodium-ion hybrid capacitors," *Journal of Materials Chemistry A,* vol. 14, no. 23, pp. 13906-13929, 2026.
[17] S. Manzeli, D. Ovchinnikov, D. Pasquier, O. V. Yazyev, and A. Kis, "2D transition metal dichalcogenides," *Nature Reviews Materials,* vol. 2, no. 8, p. 17033, 2017.
[18] D. Voiry, A. Mohite, and M. Chhowalla, "Phase engineering of transition metal dichalcogenides," *Chemical Society Reviews,* vol. 44, no. 9, pp. 2702-2712, 2015.
[19] M. A. Kamran *et al.*, "Bifunctional strontium-doped barium oxide nanorods as promising photocatalysts and electrodes for energy storage applications," *Journal of Energy Storage,* vol. 67, p. 107598, 2023.
[20] X. Xu, Q. Tian, T. Hu, D. Ji, Q. Qian, and J. Fu, "Tellurium treatment for the modification of sulfide inclusions and corresponding industrial applications in special steels: a review," *steel research international,* vol. 94, no. 5, p. 2200375, 2023.
[21] D. S. Kim *et al.*, "Synthesis and photoluminescence of Cd-doped α-MnS nanowires," *The Journal of Physical Chemistry B,* vol. 110, no. 37, pp. 18262-18266, 2006.
[22] W. Hussain *et al.*, "Synthesis of MnS from Single-and Multi-Source Precursors for Photocatalytic and Battery Applications: W. Hussain, Malik, RA Hussain, H. Hussain, Green, Marwat, Bahadur, Iqbal, Farooq, Li, and Badshah," *Journal of Electronic Materials,* vol. 48, no. 4, pp. 2278-2288, 2019.
[23] N. Li *et al.*, "Synthesis and optoelectronic applications of a stable p-type 2D material: α-MnS," *ACS nano,* vol. 13, no. 11, pp. 12662-12670, 2019.
[24] M. S. Javed *et al.*, "Tracking pseudocapacitive contribution to superior energy storage of MnS nanoparticles grown on carbon textile," *ACS Applied Materials & Interfaces,* vol. 8, no. 37, pp. 24621-24628, 2016.
[25] Y. Pei *et al.*, "Revealing the impacts of metastable structure on the electrochemical properties: The case of MnS," *Journal of Power Sources,* vol. 431, pp. 75-83, 2019.
[26] M. Z. Iqbal *et al.*, "Evaluation of d-block metal sulfides as electrode materials for battery-supercapacitor energy storage devices," *Journal of Energy Storage,* vol. 55, p. 105418, 2022.
[27] M. Almeida, A. Más, T. Silva, and M. Montemor, "From manganese oxide to manganese sulphide: Synthesis and its effect on electrochemical energy storage performance," *Electrochimica Acta,* vol. 389, p. 138711, 2021.
[28] G. Cao and Y. Wang, "Characterization and Properties of Nanomaterials. Nanostructures and Nanomaterials: Synthesis, Properties, and Applications; Volume 2 of World Scientific series in nanoscience and nanotechnology," *World Scientific: Singapore,* vol. 508, p. 581, 2011.
[29] Y. Xia *et al.*, "One-dimensional nanostructures: synthesis, characterization, and applications," *Advanced materials,* vol. 15, no. 5, pp. 353-389, 2003.